Isolating Freshwater Interface against Sea Water Intrusion and Salt Formations Using Turk Salty Concrete

Afshin. Turk[1]

[1]Khuzestan Water and Power Authority, P.O. Box 61348-13956, Ahvaz, Khuzestan, Iran; PH (+98) 916-600 2871; FAX (+98) 613-333 1001; email: a.turk@kmsu.ac.ir

ABSTRACT

Saline water causes a number of serious problems for both shoreline constructions and freshwater aquifers; whatsmore, coastal aquifers face major problems such as seawater intrusion into the interface and a decreasing in the amount of water resources during drought when water allocations from surface resources are lower less than normal. It is proposed that by injecting TSC into the interface area at a specified depth it would be possible to isolate against saline water intrusion. In 2004, huge salt domes were identified in the GOTVAND dam reservoir which could if released affect the freshwater in the Karun River. TSC grout can be used to isolate Salt formations in the form of vertical curtain. –SEM imaging at a resolution of x 2000 have shown the adhesiveness of fibers in TSC. The images show that fibers and salt concrete blend producing the ancient mummification techniques. TSC can reduce the costs and time of grouting.

INTRODUCTION

Seawater penetrates concrete coastal structures especially the piles of ports, causing damage such as skin cracking, steel bars sulfating and corrosion which manifest themselves on protective walls along the shoreline, Thompson (1987) and Chegini (2011). TSC was invented as a measure to mitigate salt formations and protect sea shorelines, Turk (2017, 2018a); whatsmore, TSC has the capability to prevent the intrusion of saline water into structures and aquifers offshore. Due to the fact that TSC materials are easily available in nature and can be used as a specific mixture per case, it is an economical solution to resolve the matter of saline water intrusion into the interface of the aquifer. It is believed that TSC can be applied in areas in the ARVAND River Estuary, and along the coastline of the Persian Gulf, conditional to the providing of funds for such projects. Grouting operations at the Interface of freshwater and seawater would then begin from 1m in shallow water (clay silt soil) to 15m in proximity to the shoreline (silt clay soil), KTNSE (2017).

TSC MATERIALS

The TSC materials used in this study were a mixture of Salt stone (S), Water (W), Cement type II or V (Cii, Cv), SHUSHTAR Ceramic Clay (C), Bentonite (B) and waste plastic fiber (F). Equation 1 defines ζ_{Turk} of TSC which is includes the existing salt water. The values of ζ_{Turk} varies from 0.75 to 6.69. Equation 2 explains the figure μ_{Turk} which is the index of salt resistance. Figure μ_{Turk} is the combination of an axial resistance of S950713 and ζ_{Turk1} at 10 days of curing. Table 1, presents ζ_{Turk}, μ_{Turk} and

Modulus of Elasticity. Figure 1 represents the behavior of materials vs the axial resistance of samples after 10 day of curing. Since 2016, samples have been taken to determine the saturation mode, KTNSE (2017). Although, the samples were broken up, all of them retained a stable shape in water. Although, the samples are broken, all of them have stable shapes in water.

Table 1. Materials Percentages of TSC, E (kg/cm²), t (days), KTNSE (2019).

i	*Sample*	*t*	*S*	*Cii,v*	*B*	*C*	*W*	*F (%)*	ζ_{Turk}	*E*	μ_{Turk}
1	950713	26	39	22v	22	0.0	17	0.0	1.30	-------	1.00
2	961222	55	40	19v	8.0	8.0	25	0.0	1.86	437	0.56
3	970216P	13	40	18ii	7.7	8.0	24	2.1	1.77	375	1.01
6	980625P	19	48	17ii	7.0	7.0	21	0.2	2.21	46,000	1.60
11	980729P	30	67	14ii	1.6	1.6	15	0.6	4.78	15,500	3.33
12	980924P	48	69	12ii	1.1	1.0	16	0.4	5.65	23,000	4.08
14	981220P	18	71	11ii	1.3	1.0	16	0.4	6.69	21,000	3.70
15	990706P	43	70	11ii	1.1	0.3	17	0.4	6.78	11,200	1.39
16	990708P	41	70	10ii	0.9	0.3	18	0.3	7.37	14,100	1.33

$$\zeta_{Turk} = (W_{Water} + W_{Salt})/(W_{Clay} + W_{Bentonite+}W_{Cement}+W_{Fibers}) \quad (1)$$

$$\mu_{Turk,i} = \frac{\sigma_i}{\sigma_{\sigma_{10,95713}}} \times \frac{\zeta_{Turk,i}}{\zeta_{Turk,1}} \, , i = 1, 2 \, , 3 \ldots \ldots \ldots , 11 \quad (2)$$

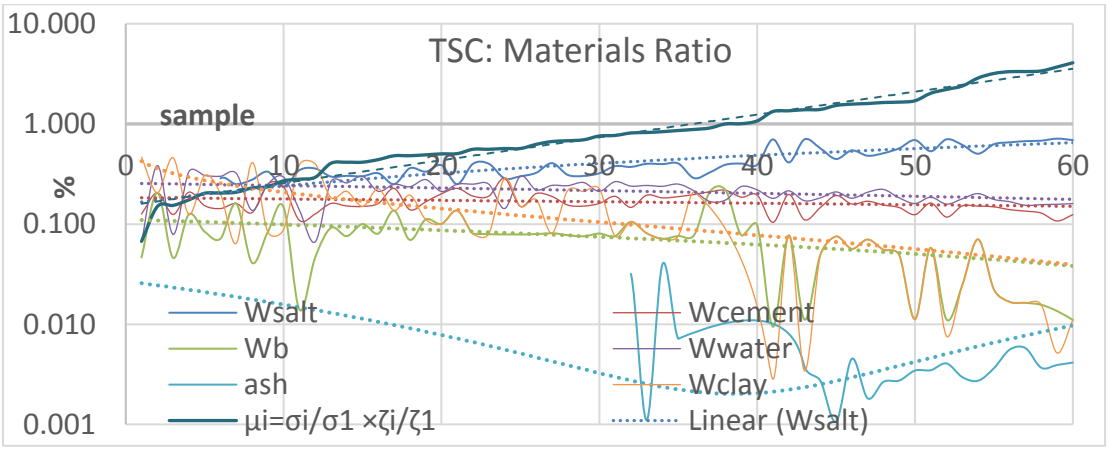

Figure 1. Index of salty resistance vs material percentage, KTNSE (2019).

Interpretation of TSC Samples

In Figure 1 the materials used in the mix such as salt, water, cement, clay, bentonite and fibers are defined. It shows the proportion of each material in the mix in terms of weight of materials which it based on the ranking of low to high values of μ_{Turk} (salt resistance index). The curve obtained for μ_{Turk} shows an increasing trend, rising up from 0.15 to 4.08 for samples. While, figure ζ_{Turk} presents a similar concurrent ascending curve. Other curves for various materials an adverse μ_{Turk} curve behavior.

$$\Delta\mu_{T_{ij}} = \mu_{T_j} - \mu_{T_i} = (\sigma_j\zeta_j)/(\sigma_1\zeta_1) - (\sigma_i\zeta_i)/(\sigma_1\zeta_1)\,, i = 1,2\,,3,\ldots\ldots j\ldots,49 \quad (3)$$

TSC- MODULUS OF ELASTICITY

The present study has shown that the mechanical properties of the TSC improved in as such that the Step Stiffness Method (SSM) was applied to analyze TSC using hydraulic jack output data figure EI (stiffness) and figure EA/L (axial stiffness). Samples were broken across the vertical axis in order to obtain a Modulus of Elasticity using the maximum tangency line of the σ-ϵ curves. The Modulus of Elasticity E_{TURK} increased by μ_{Turk} and sample curing period was up to 270 days as seen in Equations 4 to 7. The Modulus of Elasticity $f(E_Z)$ depends on the matrix E_{Turk} [3×t] in which aging (t), axial stress (σ_Z), radial stress (σ_R) and Z-Z strain (ϵ_Z) are incorporated so that when the load suddenly returns to zero the Modulus of Elasticity is recalculated, Turk(2001).

$$E_Z = (\Delta\sigma/\Delta\epsilon) = (\sigma_Y - \sigma_0)/(\epsilon_Y - \epsilon_0) \quad (4)$$

$$f(E_Z) = E_{Turk}(t, \sigma_z, \sigma_R,\ \epsilon_z\ ) = f[3 \times t_i]\,, t_i = 1,..,40,\ldots,270\ days \quad (5)$$

$$E_{Turk}(t, \sigma_z, \sigma_R,\ \epsilon_z\ ) = \begin{bmatrix} 1day & 2day & t_i & 200day & t_n \\ \sigma_{z1} & \sigma_{z2} & \sigma_{zi} & \sigma_{z200} & \sigma_{zn} \\ \sigma_{R1} & \sigma_{R2} & \sigma_{Ri} & \sigma_{R200} & \sigma_{Rn} \end{bmatrix} \quad (6)$$

$$K = (\sigma_Z\,.A)/(\epsilon_Z.L) = EA/L \quad (7)$$

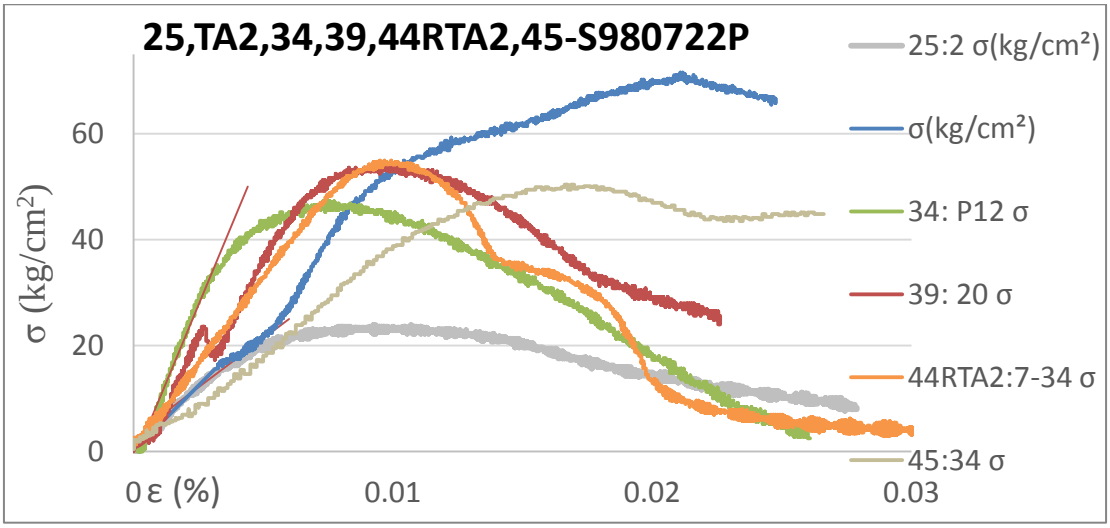

Figure 2. RTA2-44-S980722P: μ =3.19, ζ=4.08, (OCT.14.2019), KTNSE (2019).

Table 2. Figure E and Figure K of Tri-Axial and Axial: μ=2.87, ζ=2.39, S980627P.

No.	*2*	*5*	*18*	*28*	*46*
Days	7	11	*21*	33	60
E(kg/cm²)	10,909	17,857	16,464	12,500	4,472
K (t/cm)	32,452	50,829	24,238	18,402	13,577

Table 3. Figure E and Figure K of Tri-Axial and Axial: μ=2.39, ζ=3.90, S980720P.

No.	*23*	*26*	*32*	*35*	*47*
Days	1	4	*9*	14	36
E(kg/cm²)	300	2,727	6,667	7,738	10,145
K (t/cm)	702	5,797	20,423	23,254	34,230

Table 4. Figure E and Figure K of Tri-Axial and Axial: μ=3.19, ζ=4.08 S980722P.

No.	*25*	*TA2*	*34*	*39*	*44RTA2*	*45*	*51*
Days	2	7	*12*	20	34	34	37
E kg/cm^2	3,690	8,065	11,780	9,400	6,494	4,032	5,208
K (t/cm)	10,753	25,117	26,126	20,317	21,776	19,386	15,063

Table 5. Figure E and Figure K of Tri-Axial and Axial: μ=3.33, ζ=4.78, S980729P.

No.	*TA3*	*33*	*38*	*42RTA3*	*43*	*49*
Days	5	5	13	27	27	30
E(kg/cm²)	6,265	7,442	12,162	6,494	11,993	15,493
K (t/cm)	19,279	16,649	26,067	20,307	29,696	44,807

Comparison of Modulus of Elasticity in the Axial and Tri Axial Test

Figures 2 and Figure 3 show the stress- strain curves as S980722P and S980729P through which the Modulus of Elasticity is obtained through the tangency of the σ-ϵ curve. It is common for stress-strain slopes to be extended over a wide angle which in itself is used as a measure for determining a modification in TSC strength behavior. A successful behavior of axial load curves. All curves have a tendency toward the maximum slope angle. In Figure 4, TA2-S980722P7 underwent a Tri-Axial test over a 7day curing period.

Figure 4. TA2: II and Retest 44-RTA2-II-S980722P7-34 after ultimate loading.

Figure 5. Retest 42-RTA3S980729P5-27 following immersion.

TSC CRACK BEHAVIOR AND BROKEN PLANE STRESS

Figure 6 shows broken samples upon which cracks are distributed over the exterior. Tensile stress or hook stress interact along the radial plane stress. Figure 6 demonstrates the effects of the radial stress and horizontal stress σ_R which is spread along the cylindrical skin. TSC deformation is similar to the destruction of a thin-walled cylinder. Strain ϵ_R enlarges into the plastic zone without being damaged. In Figure 6, skin cracks are detailed using samples 44RTA2S980722P7-34, 43S980729P27 and 64S980729P78 respectively, which are indicative of hook stress via the waste plastic fiber.

Figure 6. Plastic fiber behavior at a ratio of 83% Salt Water in cracking spread.

Modulus of Toughness (MT) in the Axial and Tri Axial Test

TSC maximum resistance is obtained through the values obtained in the Tri Axial test. Samples are put under pressure to achieve greater strength. MT values are depended on the Tri Axial Test and μ_{Turk}. Figure 7 demonstrate that MT behavior has a correlation relationship with the values of σ_{max} and ϵ_Z. In 2018, TSC was created using the ζ_{Turk} (0.50 to 1.50). In Table 6, MT increases with σ_{max}, ϵ_Z and the curing period. In Figure 1, waste plastic fibers (F) are added.

Table 6. MT of S980729P, μ=3.33, ζ=4.78, Beer (2012), and Turk (2018a, 2018b).

No.	*TA3(5day)*	*33(5d)*	*38(13d)*	*42RTA3(27d)*	*43(27day)*	*49(30day)*
ϵ_R %	4.995	0.754	0.723	0.846	1.009	0.873
σ_{max}	66.5	34.8	49.6	32.4	68.8	53.3
MT	2.15	0.17	0.22	0.33	0.42	0.31

$$U_{TriAxial} = \int_0^{\epsilon_R} \sigma_{Rupture}.d\epsilon_Z \; ; \quad U_{AxialTest} = \int_0^{\epsilon_R} \sigma_{Rupture}.d\epsilon_Z$$

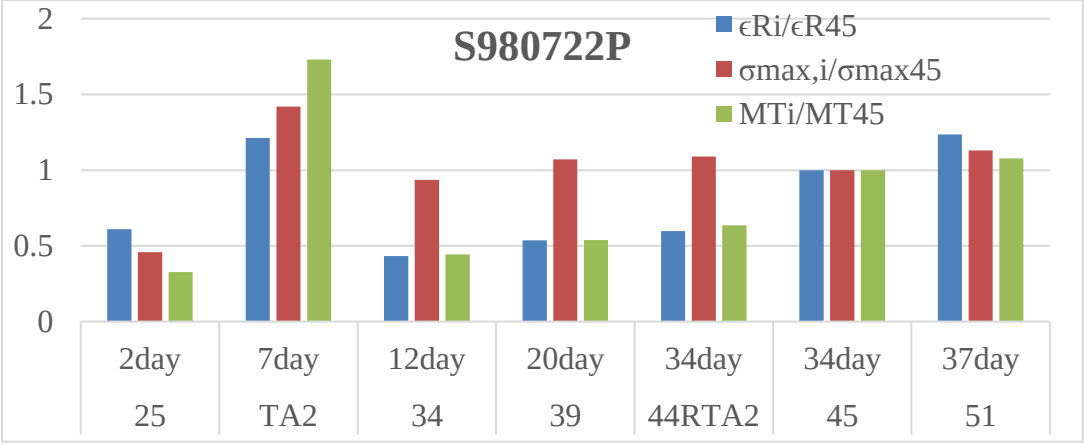

Figure 7. MT ratios for 45S980722P34, 2 to 37 days.

SSM GEOTECHNICAL ASPECTS

The step stiffness method (SSM) interprets driving pile behavior at depth using the ASTM1143 static load test, Chellis (1951). In the loading stage (Figure 8) the curve develops a convex shape and in the unloading step, the curve output appears as a multi-linear concave. These linear slopes define the axial stiffness of zones, I, II and III. The Micro pile unloading curve is divided into three zones, Turk (2004) and Ulrich (2004). Zone I is defined through the axial stiffness of soil grouting (Table 7). The modulus of Elasticity is shown in Table 7 and Table 8 respectively.

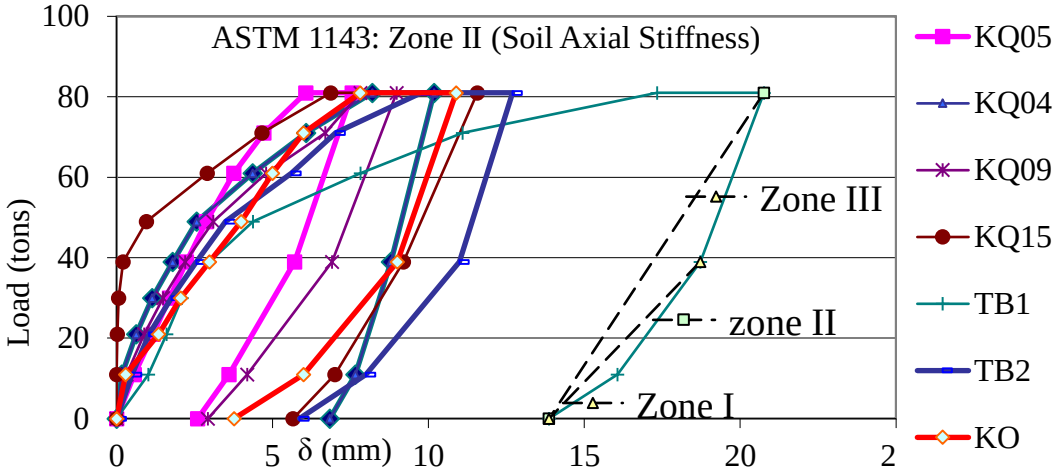

Figure 8. Driving Precast Concrete Pile, 35×35cm²×32m, Turk (2001, 2008).

$$E_{TSC}/E_{ZoneI} = \frac{26}{47} \cong \frac{1}{2}\ ;\ \ K_{TSC}/K_{ZoneII} = \frac{44}{65} \cong \frac{3}{5} \qquad (8)$$

Table 7. Micro pile Load Test, $K_{ZoneIII}$ (t/cm), E_{ZoneI} ×10³ (kg/cm²), Turk (2004).

i	*7A2*	*49L12*	*T79*	*F194*	*49L11*	*T80*	*T33*	*T2*	*F193*
$K_{ZoneIII}$	-35	-31	-26	-29	+23	+12	+23	+22	+23
E_{ZoneI}	47	63	68	109	74	118	124	157	178

Table 8. TSC Samples K_{TSC}=EA/L (t/cm), E×10³ (kg/cm²), KTNSE (2019).

No.	*X1:40C*	*12:12C*	*14:14C*	*TA1:13C*	*37RT32*	*40:32*	*30:14CF*
K_{TSC}	63	26	31	44	27	38	16
E_{TSC}	26	16	15	15	9	13	8

Table 9. Precast Concrete Pile Load Test, K_{ZoneII} = K_{Soil} (t/cm), Turk (2001).

No.	*KQ9*	*KQ5*	*TB2*	*KO*	*KQ15*	*TB1*	*KQ4*
$K_{ZoneIII}$	134	163	118	114	137	118	243
K_{ZoneII}	11	*16*	24	25	28	30	65

INTERFACE GROUTING NEAR SHORELINES

Saline water intrusion often occurs near river estuaries when the river outflow fails to prevents a backflow due to the head water potential (h) as seen in Figure 9. Equilibrium in the interface plane produces Equation 9 in the normal boundary condition, USGS (2003). If TSC grouting values are added to the equilibrium of Equation 11 then the coefficient β will be the parameter of stability for interface grouting in Equation 12. Equation 12 and Equation 13 introduce the function (h/Z) versus β, γf and γs. Figure 9 to Figure 13 demonstrate the grouting values of f(h/Z) vs the normal condition where Z=40m changes into 30m, 20m and 10m.

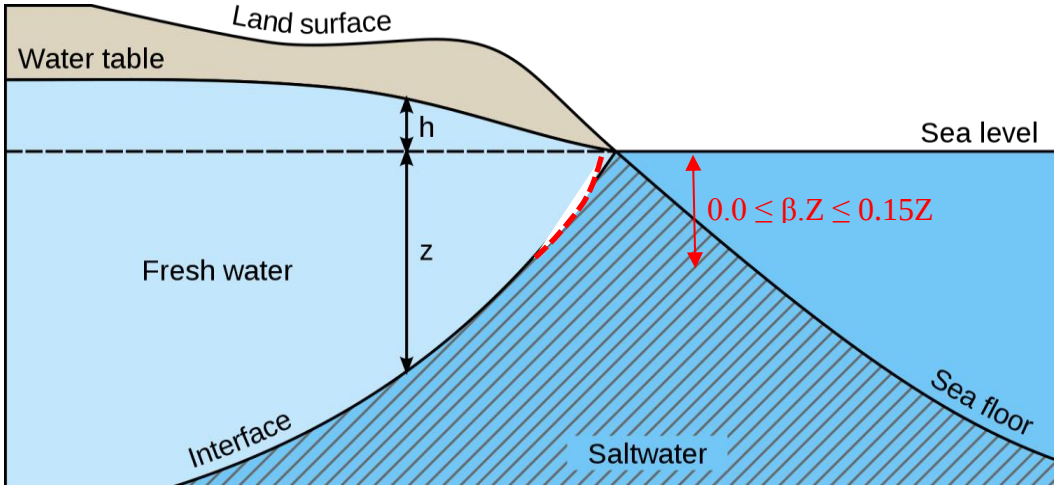

Figure 9. Grouting operating in the interface at less than β= 0.15, USGS (2003).

$$\beta = {}^{L_{grouting}}/_{Z}\ ,\ \ L_{grouting} \ll \beta Z,$$

$$\beta = 0\%,\ 5\%,\ 10\%,\ 12\%,\ 15\%$$

$$\sum_{z1=0}^{z2=h+Z} f_X = 0 \xrightarrow{Horizontal} \tag{9}$$

$$(h+Z).\gamma_{fresh} \times 1 \times \frac{1}{2}Z = \frac{1}{2}Z^2\gamma_{Salty} \tag{10}$$

$$\mathrm{f}\left(\frac{h}{Z}\right)_{Turk} = \frac{\gamma_s}{\gamma_f}(1-\beta^2) - 1 \tag{11}$$

$$^{\mathrm{h}}/_{Z} = 0.025 \quad \text{and } \beta = 0.0 \xrightarrow{Z=40m} h = 100cm$$

$$^{\mathrm{h}}/_{Z} = 0.01024 \text{ and } \beta = 0.15 \xrightarrow{Z=40m} h = 7.8cm$$

$$^{\mathrm{h}}/_{Z} = 0.01475 \text{ and } \beta = 0.10 \xrightarrow{h=20m} h = 30cm$$

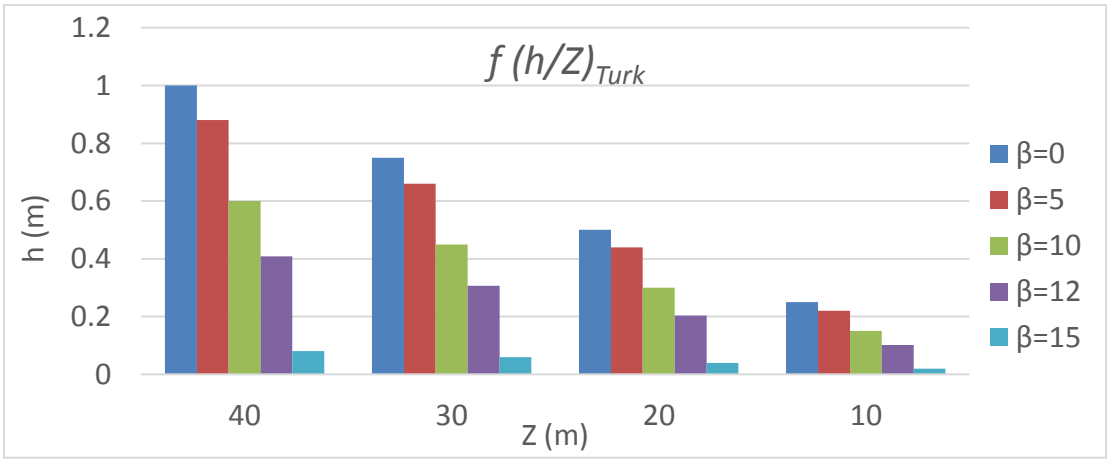

Figure 10. Comparison of *f(h/Z)* values with coefficient *β*, USGS (2003).

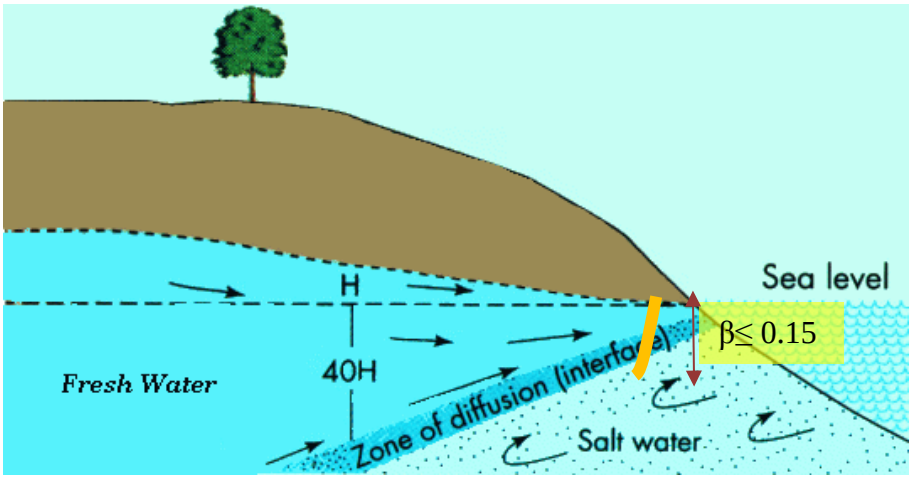

Figure 11. Zone of diffusion isolated by TSC injection, Lenntech (2021).

Equation 9 to Equation 13 conclude that TSC grouting can decrease the Z depth.

Figure 12. Salt Dome shoreline of GOTVAND reservoir will injected by TSC.

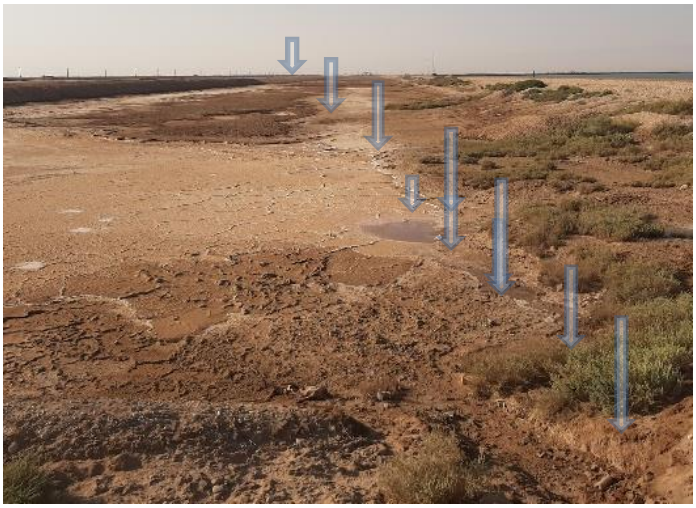

Figure 13. TSC isolation of saline water drains along KARUN River.

SEM IMAGES

Figure 14 and Figure 15 represent the SEM images of 46-S980627P60 with 0.27% plastic fiber (P), ζ_{Turk}=2.39 and a 60 day curing period. Pictures taken to study the micro behaviors of TSC adhesiveness are presented as Figure 14 which shows waste plastic fiber details at a scale of 20µm and Zone Mag= 500 X, CENLAB (2019). It appears that the plastic fibers in the TSC amalgamate with the salt crystals thus creating an entity similar to a salt mummy, the literature believe that this process might be similar to the embalming procedure used in ancient societies, Waltari (1945) and Saltmen (1993). Figure 15 shows details of salt and fiber adhesion (crystallization). The fibers merge into salt concrete in as such that the materials cannot be distinguished. Figure 15 shows a 10µm scale plastic fiber encased in salt and completely merged into it.

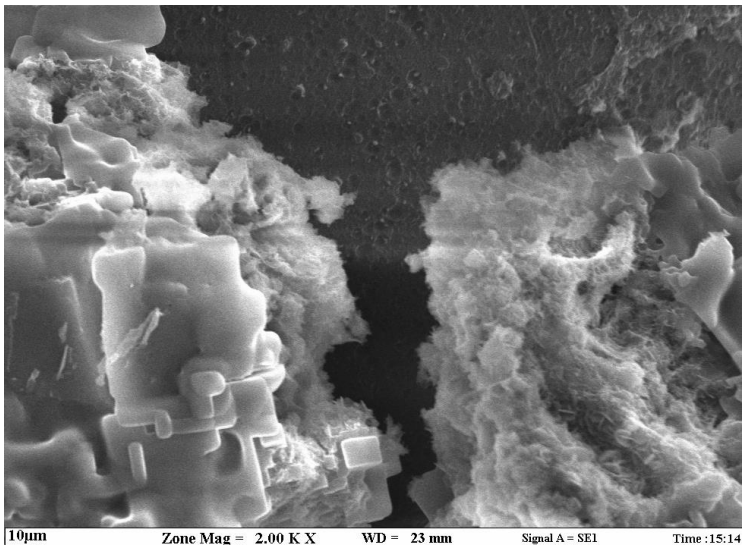

Figure 15. Mummify of plastic fibers, 46-P60, μ=2.87, ζ=2.39, CENLAB (2019).

CONCLUSION

At the beginning of the current study, ζ_{Turk} was approximately at a ratio of 0.80; however this ratio increases up to 4.1, 4.80 and 5.65 in 2019 and 5.67, 6.13 to 6.69 in 2020. These values are very significant and indicate the success of the TSC mixture design. In fact, more than 83% (to 87%) of the ingredients of TSC come from salt water whatsmore with the increase in salinity, the compressive strength of the TSC also increases, Figure 2, Figure 3, and Figure 6. The modulus of elasticity behavior is obtained through Figure 2 to Figure 3. Figure E is calculated as per Table 1 to Table 5 and Table 8. The modulus of elasticity based on its salt ratio increases. Tri-axial test pressure shows that the higher compressibility of samples greatly improves the elasticity and other properties of the TSC. It is recommended in along coastlines high-pressure grout injection be performed in several stages from low to high (1atm to 5atm); thus, TSC can be modified in shallower depths through the grouting curtains. This method can increase grout injection efficiency. TSC has the ability to repair itself after an initial crack, and will regain its initial strength after a few days. Cracks are repaired by the TSC after sliding. This fact is illustrated by Figure 2, (44RTA2, 7-34), Figure 3, (42RTA3S980729P7-27), Figure 4, Figure 5, Figure 7, Table 4, (44RTA2) and Table 8. This property is very useful in shoreline stabilization, land sliding, beach erosion and coastal protection structures. Only TSC can isolate submerged layers near beaches, along coastlines, for salt ridges, GHACHSARAN Formations (SW of IRAN) and permeable industrial and agricultural drainage canals. The total cost of TSC injection near the shoreline is less than USD $3.5 per square meter, which is an attractive economic factor for the financing of protection of freshwater aquifers. SEM images were used to show the extent of adhesion in TSC at higher resolutions. The TSC samples are remarkably mixed and difficult to separate. Plastic fiber is encased by the salt which merges with it. Salt crystallization shown through SEM imaging is indicative of the uniform arrangement of the ions.

REFERENCES

Beer, F. P. E., Johnston, R., Dewolf, jr. T., Mazurek, D. F., (2012). "Mechanic of Materials." The McGraw-Hill Companies, Inc., 6th edition.

CENLAB (2019). "SEM-Scanning Electronic Microscopic Images, TSFC Samples." Act of 2019. Pub L. No. 3CSRDFST." SHAHID CHAMRAN University of Ahvaz, Central Laboratory, LEO 417371395665VP. 98/CEN0328 IR.SCU.

CENLAB (2020). "SEM-Scanning Electronic Microscopic Images, TSFC Samples." Act of 2020. Pub L. No. 3CSRDFST." SHAHID CHAMRAN University of Ahvaz, Central Laboratory, LEO 165413990721VP. 99/CEN0323 IR.SCU.

Chegini, V., (2011). "Fundamental Design of Coastline Structures." Oceanography Center of Iran, 1th edition, Iran.

Chellis, D. R., (1951). "Pile foundation." McGraw- Hill Companies, Inc., 2th edition, Tokyo, Japan.

KTNSE, Soil Concrete Laboratory (2018), "SE Water Supply, Act of 2017. Pub L. No. 970217." KWPA. 1200/126238-K9631 IR.SE.

KTNSE, Soil Concrete Laboratory (2019), "SE Water Supply, Act of 2019. Pub L. No. 980714." KWPA. 5200/626 IR.SE.

Lenntech (2020). "Seawater intrusions in groundwater"< https://www.lenntech.com/groundwater/seawater-intrusions.htm>

Saltmen (1993). "Iran National Museum". < https://en.wikipedia.org/wiki/Saltmen>

Thompson, P.; Penning-Rowsell, E. C.; Parker, D. J; and Hill, M. I., (1987). "Interim Guidelines for Economic of Coast Protection and Sea Defense Schemes", flood hazard res. Center, Middlesex polytechnic.

Turk, A., (2001). "Driving Force by Kpile Method and Pile Loading Test, Concrete Piles ", CSCE, Canada.

Turk, A. and Zaemeri, A. A., (2004). "Micro pile behaviors study using compressive (or tensile) pile load test and step stiffness method", CSCE, Canada.

Turk, A.; Salehi, F.; Kolahchi, A.; Ghanavatizadeh, S., (2007). "Elasticity Module of Karkheh Earth Dam Study & Behavior through Inclinometers & SSM", Proc., Int. ISEC-04, Melbourne, Australia.

Turk, A., Ghanavatizadeh, S., Zaamari, A.A., Kolahchi, A., (2008). "Regeneration of Missed Record Data, Vertical Axes of Karkheh Earth Dam Using Cell Pressure, Mathematical Aspects and SSM", ASCE Aerospace Division, USA.

Turk, A., Mombeni, B., Bahmaei, D., Khodabakhshi, H. R., Behdarvandi, A. M., and Ghanavatizadeh, S., (2017). "Coastal Protection of GOTVAND Reservoir DAM, EC Perfection of Salty Domes." Proc., Int. ISEC-09, Valencia, Spain, 10.14455/ISEC.res.2017.61.

Turk, A., (2018). "Stabilization of Pure Salty Formations of the GOTVAND Dam Lake and another Salty Drought Desert Regions through Invention of Turk Salty Mortar ", ASCE Aerospace Division, USA.

Turk, A., Mombeni, B., Afrasiabi, S., and Ghanavatizadeh, S., (2018). "Turk Salty Mortar through Addition of Plastic and Cotton Waste Materials to stabilize problematic Coastlines." ISEC Press, Australia, 10.14455/ISEC.res.2018.135.

USGS (2003). "Salt water intrusion"<https://pubs.usgs.gov/circ/2003/circ1262/#figurecaption54419776>

Waltari, M., (1945) "Sinuhe Egyptiläinen". WSOY Press, Finland.